Journal of Biomechanics 159 (2023) 111758

Contents lists available at ScienceDirect

Journal of Biomechanics

journal homepage: www.elsevier.com/locate/jbiomech

Comparative validation of two patient-specific modelling pipelines for predicting knee joint forces during level walking

Domitille Princelle, Giorgio Davico *, Marco Viceconti

Medical Technology Lab, IRCCS Istituto Ortopedico Rizzoli, Bologna, Italy
Department of Industrial Engineering, Alma Mater Studiorum - University of Bologna, Italy

ARTICLE INFO

Keywords:
Musculoskeletal model
Subject-specific model
Image-based model
Joint Load
Predictive accuracy

ABSTRACT

Over the past few years, the use of computer models and simulations tailored to the patient's physiology to assist clinical decision-making has increased enormously. While several pipelines to develop personalized models exist, their adoption on a large scale is still limited due to the required niche computational skillset and the lengthy operations required. Novel toolboxes, such as *STAPLE*, promise to streamline and expedite the development of image-based skeletal lower limb models. *STAPLE*-generated models can be rapidly generated, with minimal user input, and present similar joint kinematics and kinetics compared to models developed employing the established *INSIGNEO* pipeline. Yet, it is unclear how much the observed discrepancies scale up and affect joint contact force predictions. In this study, we compared image-based musculoskeletal models developed (i) with the *INSIGNEO* pipeline and (ii) with a semi-automated pipeline that combines *STAPLE* and nmsBuilder, and assessed their accuracy against experimental implant data. Our results showed that both pipelines predicted similar total knee joint contact forces between one another in terms of profiles and average values, characterized by a moderately high level of agreement with the experimental data. Nonetheless, the Student *t-test* revealed statistically significant differences between both pipelines. Of note, the *STAPLE*-based pipeline required considerably less time than the *INSIGNEO* pipeline to generate a musculoskeletal model (i.e., 60 vs 160 min). This is likely to open up opportunities for the use of personalized musculoskeletal models in clinical practice, where time is of the essence.

1. Introduction

There are several clinical problems where knowing the force being transmitted at the patient's joints during stereotypical tasks, such as level walking, would be paramount (Erdemir et al., 2007; Fraysse et al., 2009; Martelli et al., 2011; Pedersen et al., 1997; Viceconti et al., 2019). Unfortunately, intersegmental and internal forces can only be measured *in vivo* through instrumented implants (Bergmann et al., 2001; Brand et al., 1994; Fregly et al., 2012; Kim et al., 2009; Taylor et al., 2017, 2004) or invasive tendon sensors (Bull et al., 2005; Finni et al., 1998; Komi et al., 1992) that for ethical reasons are seldomly used. Moreover, by definition, the invasiveness of the above procedures alters the system being observed. Alternatively, musculoskeletal (MSK) models may be employed to non-invasively predict joint contact forces both in healthy individuals (Hamner et al., 2010; Saxby et al., 2016) and patients (Barber et al., 2017; Davico et al., 2020b; Falisse et al., 2019; Montefiori et al., 2019).

Since their introduction in the 1970s (Morrison, 1970; Seireg and Arvikar, 1973), pipelines and workflows to generate MSK models have evolved considerably. Generic models built off template anatomies representative of healthy adults (Brand et al., 1994; Carbone et al., 2015; Delp et al., 1990; Garner and Pandy, 2001; Hamner et al., 2010; Klein Horsman, 2007; Rajagopal et al., 2016) remain largely employed. However, their simple anthropometric scaling to better approximate the size of the subject under study has been questioned. Generic geometries were found to be not very accurate when compared to medical imaging data (Davico et al., 2020a; Suwarganda et al., 2019). Moreover, muscle properties do not scale linearly with bone geometries and differ between individuals (Ward et al., 2009). Thus, highly detailed subject-specific MSK models generated from medical images were introduced (Arnold et al., 2000; Barzan et al., 2019; Scheys et al., 2005; Taylor et al., 2017). Subject-specific models were consistently shown to be more accurate than generic models in estimating joint kinematics and kinetics (Kainz et al., 2016; Wesseling et al., 2016), muscle moment arms (Scheys et al., 2008), and joint contact forces (Gerus et al., 2013; Lenaerts et al., 2008; Marra et al., 2015; Wesseling et al., 2016). However, personalization

* Corresponding authors at: Medical Technology Lab, IRCCS-Istituto Ortopedico Rizzoli, Via di Barbiano 1/10, 40136 Bologna, Italy.
E-mail addresses: domitille.princelle@unibo.it (D. Princelle), giorgio.davico@unibo.it (G. Davico).

https://doi.org/10.1016/j.jbiomech.2023.111758
Accepted 7 August 2023
Available online 9 August 2023
0021-9290/© 2023 The Authors. Published by Elsevier Ltd. This is an open access article under the CC BY-NC-ND license (http://creativecommons.org/licenses/by-nc-nd/4.0/).

comes at a cost. The process of developing a subject-specific MSK model is not straightforward and requires time, which adds up to the time required to collect and process relevant experimental and imaging data, and manage the patients.

Despite the availability of software and workflow to streamline and standardize the procedure (Correa et al., 2011; Killen et al., 2021; Marra et al., 2015; Nardini et al., 2020; Taddei et al., 2012; Zhang et al., 2014), developing subject-specific models remains time-consuming (Arnold et al., 2000; Modenese et al., 2018; Scheys et al., 2005). For example, the *INSIGNEO* pipeline, proposed by Modenese et al., (2018), requires up to 10 h to generate a full lower limb MSK model and has only been used in a few studies (Montefiori et al., 2019; Viceconti et al., 2019). More recently, the *STAPLE* toolbox was released and promised to fully automate the generation of a skeletal model (i.e., bones and joints) without losing accuracy (compared to models developed using the *INSIGNEO* pipeline) (Modenese and Renault, 2021). Muscles, however, are not automatically included in *STAPLE*-generated models. Hence all comparisons were limited to joint kinematics and kinetics. Therefore, we hereby present a semi-automated pipeline combining *STAPLE* (for the skeletal model) and nmsBuilder (Valente et al., 2017) (to define muscle pathways) for the rapid generation of personalized full-lower limb MSK models.

This work aimed to compare MSK models developed following the *INSIGNEO* pipeline and the *STAPLE*-based pipeline in terms of predictive accuracy to demonstrate the validity of the latter. To do so, the tibiofemoral joint contact force predicted by subject-specific MSK models, built using the two pipelines, were compared (i) against the corresponding experimental data (instrumented implant) and (ii) against one another.

2. Materials and methods

2.1. Experimental data

Experimental data on four elderly subjects implanted with an instrumented knee prosthesis (Table 1) were obtained from the last four editions of the "Grand Challenge Competition to Predict In Vivo Knee Loads" (hereinafter KGC for short) (Fregly et al., 2012). Specifically, the datasets included (i) lower-limb CT scans and segmented geometries of the pelvis, femur, tibia, fibula, talus, calcaneus, and toes, (ii) 3D reconstruction of the implant components, (iii) motion capture, electromyography, and force plates data, and (iv) the continuous recordings of the instrumented knee implant acquired while the subjects performed various locomotor tasks (e.g., level-ground walking).

Overall, nineteen gait trials were analyzed (Table 1). Motion capture data were processed in MATLAB® (R2021b, The MathWorks Inc., Natick, Massachusetts) using MOtoNMS (Mantoan et al., 2015). Specifically, the ground reaction force and motion capture data for each gait trial (i.e., between consecutive heel strikes of the instrumented leg) were low-pass filtered with a zero-lag fourth-order Butterworth filter with a cut-off frequency of 8 Hz.

Incomplete geometries, e.g. pelvis, were reconstructed using statistical shape modelling techniques via the MAP Client (Zhang et al., 2014). On the other hand, missing geometries, such as toes or calcaneus, were extracted from the generic Full Body model (Rajagopal et al., 2016) and scaled to the participant's dimensions in OpenSim (v4.1).

Table 1
Anthropometrics of the four subjects included in the study.

	3rd	4th	5th	6th
Gender	Female	Male	Male	Male
Age	68	86	NaN	86
Prosthesis side	Left	Right	Left	Right
Mass (kg)	78.4	66.7	75	70
Height (cm)	167	168	180	172
Gait trials	5–6–7–8	2–3–4–5–7	1–8–9–11	3–4–5–6–7–9

2.2. Modelling methods

Starting from the available imaging data, two single-leg subject-specific models were built for each subject (i.e., eight models in total), employing (i) the *INSIGNEO* pipeline (Modenese et al., 2018) and (ii) a novel pipeline that combines the *STAPLE* toolbox (Modenese and Renault, 2021) and nmsBuilder (Valente et al., 2017, 2014). Of note, the two pipelines differ in the procedure to generate the skeletal model, while muscles are introduced and personalized analogously.

The generated MSK models were made of 7 segments (pelvis, thigh, patella, shank, talus, calcaneus, and toes), 13 degrees of freedom and 40 muscles. The pelvis was connected to the ground with a free joint, the hip joint was idealized as a ball-and-socket joint, the knee, ankle, subtalar, and metatarsophalangeal joints were idealized as hinges, and the patellofemoral joint was coupled with the knee joint (as detailed in the section below).

2.3. Skeletal model

- *INSIGNEO* pipeline

Using the *INSIGNEO* pipeline, described in detail in a step-by-step guideline (Modenese et al., 2018), the kinematic chain was built using analytical shapes that approximated the articular surfaces of the bones. Specifically, the dimensions and locations of the analytical shapes (i.e., cylinders and spheres) provided the parameters to define the anatomical joint reference systems (i.e., the location of the center and axes orientation). For example, the knee joint center was defined as the mid-point between the centers of two spheres fitting the femoral condyles, which were further used to define the mediolateral axis (as the line connecting the two centers). Then, the vertical axis was identified along the line connecting the previously identified knee and hip joint centers. Finally, the right-hand rule identified/indicated the anterior-posterior axis (Modenese et al., 2018; Wu et al., 2002). For the toes joint, the reference system was built upon manually selected anatomical landmarks.

Once the kinematic chain was created, the single-leg OpenSim model was generated by assigning the appropriate densities (Dumas et al., 2005; White et al., 1987). The entire process was performed in the nmsBuilder freeware (Valente et al., 2017, 2014).

- *STAPLE*

STAPLE is a shared tool still under development. The version used in this study was the latest available at the time (v. beta3) on the SimTK website (https://simtk.org/projects/msk-staple). *STAPLE* requires the same input information as nmsBuilder, i.e., segmented bones and mass of the subject. From there, the toolbox automatically generates the skeletal model. The process is based on a morphological analysis of the bones performed using different algorithms (GIBOC (Renault et al., 2018), *STAPLE* (Modenese and Renault, 2021) and Kai (Kai et al., 2014)). Specifically, the GIBOC algorithms were used for the hip and knee joints (GIBOC-sphere), while the *STAPLE* algorithms were used for the ankle and subtalar joints. The anatomical landmarks and points, thus identified, were subsequently used to define the coordinate systems. In less than 30 s, *STAPLE* generated a single-leg OpenSim skeletal model.

2.4. Patellofemoral joint

All models developed in this study featured a patellofemoral joint with a 3D motion but one degree of freedom (Arnold et al., 2010; Rajagopal et al., 2016). Specifically, the patellofemoral joint was modelled as a custom joint, where the transversal and frontal rotations were not allowed (Arnold et al., 2010; Rajagopal et al., 2016). The mediolateral rotation axis was identified using a cylinder that fitted the articular surfaces, recognized as the trochlea and intercondylar space, identified on the implant component. The three translational motions of

the joint were defined using splines extracted from the literature (Arnold et al., 2010; Rajagopal et al., 2016) that were scaled to the patient using palpated anatomical landmarks and modified such that the patella articulated with the femur (Viceconti et al., 2019). The splines were parameterized to enable a 3D motion of the patella during the flexion–extension motion. In addition, through the patellar tendon, the quadriceps muscles, wrapped around the patella, were attached to the tibia. Mechanically, the quadriceps muscle forces were transmitted through the patellar tendon during the tibiofemoral motion. Finally, the patellofemoral joint motion was coupled with the tibiofemoral joint angle, which enabled the patella to move in dependence on the tibiofemoral joint angle. This mechanism allowed for an estimation of knee contact forces in good agreement with experimental data (Lerner et al., 2015; Rajagopal et al., 2016; Viceconti et al., 2019).

2.5. Musculotendon parameters

The coordinates of the path points (origin, insertion and via points) for all 40 muscles, initially extracted from the generic Full Body model (Rajagopal et al., 2016), were mapped onto the segmented bone geometries using a single-value decomposition algorithm and affine transformations (Horn, 1987). The transformation matrix applied to all muscle points was the transformation matrix that enabled to register a subset of anatomical landmarks identified on the reference generic models to the corresponding points on the segmented geometries (Modenese et al., 2018). The mapped muscle points were then visually inspected against the CT scans, and minimal adjustments were performed if point locations were deemed unsatisfactory (e.g., muscle points inside the bone). Where needed, wrapping surfaces were further introduced to ensure physiological muscle behavior (e.g., to avoid in-bone penetration). Independently on the pipeline employed, the muscle points were mapped following the above procedure. Nonetheless, the final position of each muscle point might have differed (RMSE = 3.4 ± 3.6 mm, a maximum distance of 21.2 mm and a minimum distance <0.1 mm – Annex 1). The transformation matrix was, in fact, determined from a subset of anatomical landmarks, whose location on the bony geometries may have differed when identified manually (nmsBuilder*)* or automatically (*STAPLE*) (RMSE = 7.1 ± 3.4 mm, with a maximum distance of 13.6 mm and a minimum distance <0.1 mm – Annex 1).

Muscle parameters (i.e., pennation angle, optimal fibre length, and tendon slack length) were initially extracted from the generic Full Body model (Rajagopal et al., 2016) scaled to each patient's dimensions. Then, the optimal fibre and tendon slack lengths values were morphometrically optimized (Modenese et al., 2016). For each participant, the maximal isometric force of each muscle was scaled with the ratio between the total lower-limb muscle volume extracted from the CT scans and the corresponding quantity proper of the generic Full Body model (Rajagopal et al., 2016), which was back-calculated from the generic muscle parameters. The maximal isometric force was further personalized for the quadriceps muscle using the muscle volumes individually segmented on the CT scans. For one participant (KGC3), who was an older woman, a dataset of muscle volumes reflecting the participant's age and physiology was used (Montefiori et al., 2020). In particular, the upper range of the muscle volumes in the dataset (one standard deviation above the average) was used to personalize the maximal isometric force of 19 muscles.

Each model generation step (except the segmentation) was timed for both pipelines to quantify the effort required to generate a complete MSK model.

2.6. Biomechanical simulations

Within OpenSim 4.1 (Delp et al., 2007; Seth et al., 2018), the eight subject-specific MSK models were employed to run biomechanical simulations of gait to predict the tibiofemoral contact forces.

Firstly, the Inverse Kinematics tool was used to compute joint coordinates by solving a weighted least square problem that minimizes the distance between corresponding pairs of experimental and virtual markers (Lu and O'Connor, 1999). Then, an Inverse Dynamic analysis was performed to predict the external torques acting on the joints. Next, the Static Optimization tool was used to estimate muscle forces, enforcing the force–length-velocity relationship. The muscle redundancy problem was solved by minimizing the sum of squared muscle activations (Anderson and Pandy, 2001; Crowninshield and Brand, 1981). Ideal moment generators (i.e., reserve actuators), which supported the muscles in counterbalancing the external joint moments, were added solely to the hip joint. To minimize the contribution of these ideal moment generators, their optimal force was set to a value ≤8Nm. Finally, a Joint Reaction Analysis was conducted to estimate the joint contact forces components acting on the tibia.

2.7. Data analysis

First, the skeletal models automatically generated were compared against those manually created by reporting the differences in the joint coordinate systems' origins' location and axes orientation. Then, the average tracking error during the inverse kinematic, i.e., the total squared error, the root mean squared error (RMSE) and the maximal error ($Error_{Max}$), were reported for both pipelines and each participant.

Both the predictions and the recordings of the instrumented implants were converted into a total contact force to enable direct comparisons. Then, predicted and experimental knee joint contact forces were interpolated to 101-point vectors to be expressed as a percentage of the gait cycle, and normalized to body weight (BW). The analysis was based on two metrics commonly employed to quantify the level of agreement between profiles, i.e. the RMSE and the coefficient of determination (R^2), computed between experimental recordings and corresponding model knee contact force predictions.

A factorial analysis was conducted to assess whether the models' predictive accuracy was dependent on the subject or model under study. Finding no differences would allow the 19 trials to be grouped together, thus increasing the sample size for statistical power.

Finally, the R^2 and RMSE were computed between the predicted knee contact forces, and one-sample Student's one-tailed *t-test* was performed to determine whether the two modelling pipelines produced similar results (i.e., mean RMSEs equal to 0 BW and R^2 equal to 1, with α set to 0.05).

3. Results

The average time to develop a subject-specific MSK model using the *STAPLE*-based pipeline was 60 min, less than the time required with the *INSIGNEO* pipeline (i.e., 160 min) (Table 2).

Overall, the two pipelines generated highly similar skeletal models (Table 3). For each subject, the location of the origin of the joint reference systems did not vary considerably between pipelines. In particular, the average distance between corresponding origins across subjects was smaller than 8 mm for each joint coordinate systems (i.e., 6.3 ± 2.5 mm for the pelvis-ground joint, 1.3 ± 1.4 mm for the hip joint, 6.1 ± 2.7 mm for the knee joint, 4.5 ± 4.9 mm for the ankle joint and 8.0 ± 7.2 mm for the subtalar joint). However, differences as large as 17.7 mm and 13 mm were observed for the subtalar joint (KGC5) and for the ankle joint (KGC6), respectively.

All models were able to properly track experimental markers with

Table 2
Average time required to develop the skeletal model and to perform the muscle registration using the two pipelines.

Pipeline	Skeletal model	Muscle geometries	Complete model
INSIGNEO	~100 min	~60 min	~160 min (~2 h 40 min)
STAPLE + nmsBuilder	30 s		~60 min

Table 3
Differences in the joint coordinate systems origin placement and axes orientation between the STAPLE-based and INSIGNEO models. Linear distances between the origins of the joint coordinate systems are expressed in the reference system of the medical images, for which the axes directions are Z pointing cranially, Y posteriorly, and X to the left for each participant.

KGC	Joint	Origin displacement vector (mm)				Differences in the orientation of the axes – Parent (°)			Differences in the orientation of the axes – Child (°)		
		X	Y	Z	Norm	X	Y	Z	X	Y	Z
KGC3	Pelvis-ground	<0.1	0.1	−4.2	4.2	<0.1	<0.1	<0.1	9.2	−5.6	<0.1
	Hip	−0.1	−1.8	3.1	3.6	−6.0	−1.1	−8.9	<0.1	<0.1	<0.1
	Knee	0.8	−6.0	−8.6	10.5	13.5	2.2	−0.6	13.5	2.2	3.9
	Ankle	−1.4	−0.3	−0.4	1.5	−0.4	−1.6	−1.2	−0.4	−1.6	1.1
	Subtalar	0.4	−0.8	−0.9	1.3	−5.1	−1.4	−17.1	−5.1	−1.4	−17.1
KGC4	Pelvis-ground	−0.9	−2.6	7.9	8.3	<0.1	<0.1	<0.1	−17.0	8.9	−17.5
	Hip	0.4	0.1	1.0	1.1	2.6	−0.4	6.4	−1.3	−1.3	0.8
	Knee	−1.3	−3.0	2.2	3.9	2.6	−1.6	−3.0	2.6	−1.6	−3.0
	Ankle	0.2	−1.4	2.2	2.6	−1.0	−0.3	−1.2	−1.1	−0.3	−3.0
	Subtalar	0.0	−0.5	0.7	0.8	5.8	−4.5	1.4	5.8	−4.5	1.4
KGC5	Pelvis-ground	−2.9	1.0	−1.8	3.6	<0.1	<0.1	<0.1	12.9	5.2	38.2
	Hip	−0.1	−0.1	0.2	0.2	11.6	−2.6	−37.9	10.3	−3.9	12.1
	Knee	1.0	3.6	1.1	3.9	33.0	−3.5	23.1	33.0	−3.5	12.1
	Ankle	−0.3	−0.5	−0.9	1.1	−1.4	−1.4	−1.0	−1.4	−1.4	2.2
	Subtalar	6.0	13.3	10.0	17.7	12.2	−3.0	−3.7	12.2	−3.0	−3.7
KGC6	Pelvis-ground	6.4	3.4	−5.9	9.3	<0.1	<0.1	<0.1	<0.1	−5.7	3.4
	Hip	0.2	−0.3	0.2	0.4	<0.1	<0.1	<0.1	<0.1	<0.1	<0.1
	Knee	−0.4	5.6	2.1	6.0	6.2	0.6	−7.0	6.2	0.4	−5.4
	Ankle	3.4	−12.1	3.3.	13.0	−6.4	6.9	−2.3	−6.4	6.9	2.9
	Subtalar	5.1	−9.6	5.4	12.2	−3.5	5.0	2.1	−3.5	5.0	2.1

Table 4
Inverse kinematic tracking errors, expressed as mean and standard deviation across the various trials, for all the developed models. The error between corresponding virtual and experimental markers was computed in terms of squared error, RMSE and maximal error ($Error_{Max}$).

	INSIGNEO			*STAPLE* + nmsBuilder		
	Squared error (cm)	RMSE (cm)	$Error_{Max}$ (cm)	Squared error (cm)	RMSE (cm)	$Error_{Max}$ (cm)
KGC 3	0.9 ± 0.3	2.2 ± 0.4	3.3 ± 0.5	0.5 ± 0.1	1.7 ± 0.2	3.1 ± 0.2
KGC 4	0.1 ± 0.03	0.6 ± 0.1	1.1 ± 0.2	0.5 ± 0.03	1.7 ± 0.1	3.4 ± 0.1
KGC 5	0.1 ± 0.04	0.8 ± 0.1	2.1 ± 0.3	0.3 ± 0.04	1.1 ± 0.1	2.7 ± 0.2
KGC 6	0.5 ± 0.2	1.8 ± 0.1	3.6 ± 0.3	0.8 ± 0.2	2.0 ± 0.2	3.8 ± 0.3
All KGC	0.4 ± 0.1	1.3 ± 0.2	2.5 ± 0.3	0.6 ± 0.1	1.7 ± 0.1	3.4 ± 0.2

errors below the validity threshold of OpenSim best practices ($Error_{Max}$ = 3.4 ± 0.2 cm for the *STAPLE*-based pipeline and $Error_{Max}$ = 2.5 ± 0.3 for the *INSIGNEO* pipeline - Table 4).

The factorial analysis showed no significant differences (χ^2 = 0.064574, $d_f = 1$, $p = 0.746$) for both RMSE and R^2, revealing that the differences in predicted knee joint contact forces could not be attributed to the patient nor the model. Based on these results, all data were pooled together. RMSEs and R^2 values were reported as the average across the 19 analyzed trials for the remaining analyses.

In terms of predicted knee contact forces, both modelling pipelines' results were close to the reference measured values with an RMSE of 0.38 ± 0.11 BW (ranging from 0.21BW to 0.59 BW) and 0.40 ± 0.09 BW (ranging from 0.27 BW to 0.61 BW) for the *INSIGNEO* and *STAPLE*-based pipeline, respectively (Table 5). Similarly, the R^2 values showed a moderately high level of agreement between experimental and predicted forces (i.e., R^2 = 0.89 ± 0.06 for the *INSIGNEO* pipeline; R^2 = 0.88 ± 0.05 for the *STAPLE*-based pipeline) (Fig. 1).

Compared to one another, the two modelling pipelines produced highly similar knee contact force profiles, with average RMSE and R^2 values (across 19 trials) respectively smaller than 0.20 BW (0.20 ± 0.07 BW) and larger than 0.97 (0.97 ± 0.02) (Fig. 2). Nonetheless, the hypothesis that the *INSIGNEO* and the *STAPLE*-based pipelines produced non-significantly different predictions was rejected by the Student's *t-tests*. In particular, the mean values were found to be significantly different from the ideal value of 0 for the RMSE (t = 11.68, p = 3.85e−10) and 1 for R^2 (t = 6.23, p = 3.52e−06).

Table 5
Mean and standard deviation of the RMSE, expressed in body weight (BW), and R^2 of the predicted knee contact forces for each KGC edition of each pipeline against the experimental data.

	INSIGNEO		*STAPLE* + nmsBuilder	
	RMSE (BW)	R^2	RMSE (BW)	R^2
KGC 3	0.36 ± 0.03	0.93 ± 0.03	0.36 ± 0.05	0.89 ± 0.05
KGC 4	0.37 ± 0.06	0.90 ± 0.03	0.39 ± 0.02	0.88 ± 0.04
KGC 5	0.25 ± 0.03	0.96 ± 0.01	0.30 ± 0.02	0.93 ± 0.01
KGC 6	0.50 ± 0.08	0.83 ± 0.05	0.48 ± 0.09	0.85 ± 0.05
All KGC	0.38 ± 0.11	0.89 ± 0.06	0.40 ± 0.09	0.88 ± 0.05

4. Discussion

This study aimed to show the predictive accuracy of subject-specific MSK models developed using a semi-automated *STAPLE*-based pipeline compared to the *INSIGNEO* pipeline (Modenese et al., 2018). Experimental data from four elderly subjects implanted with an instrumented total knee prosthesis were processed and employed to evaluate the proposed methodology. Overall, eight MSK models (one per subject and pipeline) were built off each subject's medical imaging data collected in the last four editions of the KGC competition (Fregly et al., 2012).

In line with previous work, all developed models – independently of the pipeline used – predicted total knee joint contact forces in good agreement with the experimental values measured during level walking (i.e., RMSE of 0.38 ± 0.11 BW and R^2 = 0.89 ± 0.06 using the *INSIGNEO* pipeline; RMSE = 0.40 ± 0.09 BW and R^2 = 0.88 ± 0.05 using the *STAPLE*-based pipeline). Moreover, the values and shape of the predicted contact forces approximated those reported in the literature on the same dataset (Bennett et al., 2022; Marra et al., 2015; Thelen et al., 2014). Specifically, the observed RMSE values were lower than the average errors reported by Thelen et al., (2014) (i.e., RMSE = 0.51 BW) but slightly higher than those reported by Marra et al., (2015) (i.e., RMSE =

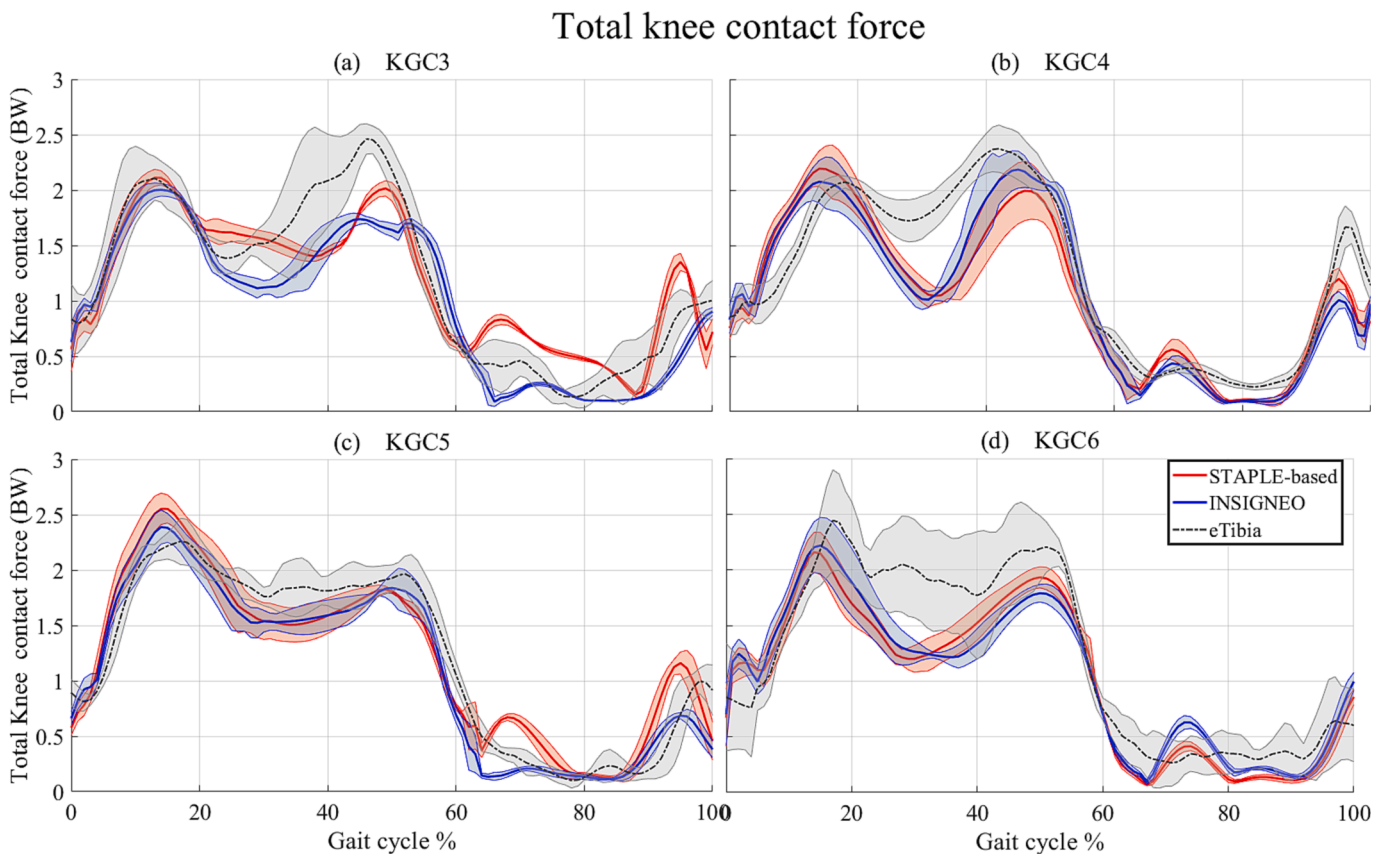

Fig. 1. Mean (line) and standard deviation (shaded area) of the total knee contact force, expressed in body weight (BW), for the experimental data *eTibia* (black, dotted-line), and those predicted by the model generated by the *INSIGNEO* (blue) and the *STAPLE*-based (red) pipeline for each KGC edition (a–d). (For interpretation of the references to colour in this figure legend, the reader is referred to the web version of this article.)

0.30 BW) for KGC4 and KGC5 respectively (Table 5). Various factors could contribute to these differences, including how the models were generated (generic model (Thelen et al., 2014) versus subject-specific as in the present study and in Marra et al., 2015), their complexity (e.g., patellofemoral joint, ligament, and contact models (Marra et al., 2015; Thelen et al., 2014) and the muscle properties (e.g., the maximal isometric force determined by muscle volume (Marra et al., 2015)).

Comparing the two pipelines to one another in terms of predicted knee joint contact force profiles, we observed an excellent level of agreement (i.e., RMSE = 0.20 ± 0.07 BW; R^2 = 0.97 ± 0.02). However, in contrast to our hypothesis, the Student's *t-test* found the RMSE to be significantly higher than 0 BW (i.e., perfect overlap) and the R^2 value significantly lower than the maximum (i.e., 1). This minimal, yet statistically significant, difference could be due to several factors. For instance, the minor discrepancies observed in the marker set (location of anatomical landmarks) and in the location of the joint reference systems between models developed in nmsBuilder or *STAPLE* may have played a role. However, Modenese and Renault (2021) previously reported negligible kinematic and kinetic differences between skeletal models manually developed with the *INSIGNEO* pipeline and those automatically generated with the *STAPLE*-based pipeline. Similarly in the present study, the location of the joint reference systems (origin) in the skeletal models developed with the two tested pipelines were comparable (Table 3). In addition, the inverse kinematic tracking errors were within the acceptability threshold as per OpenSim best practices, i.e., a maximal error less than 2–4 cm and the RMSE under 2 cm (Table 4), and the predicted kinetics presented negligible differences (Supplementary data). Muscle points were mapped onto the bony geometries using the same methodology for both pipelines. However, the transformation matrix employed in the mapping procedure differed between pipelines since it was determined from anatomical landmarks whose location varied between the two (RMSE = 7.1 ± 3.4 mm, a maximum distance of 13.6 mm and a minimum distance <0.1 mm – Annex 1). As a result, minor discrepancies were also observed in the muscle pathways between pipelines, specifically in the location of the muscle landmarks (RMSE = 3.4 ± 3.6 mm, a maximum distance of 21.2 mm and a minimum distance <0.1 mm – Annex 1). Such differences, considered in the range of human error and human inter-operator repeatability (Martelli et al., 2015), may have affected muscle moment arm calculations, muscle function (i.e., muscle forces and activations), and joint contact loads (Martelli et al., 2015; Valente et al., 2014).

The key feature of the presented semi-automated approach resides in the ease and small effort required to generate subject-specific image-based MSK models. Indeed, according to Modenese et al., (2018), the development of a single-leg skeletal model using the *INSIGNEO* pipeline takes an average of 2 h (starting from the segmented bones), which is in line with the time recorded in the study (approximately 100 min for the skeletal model). On the other hand, the single-leg skeletal model is generated in less than 30 s using *STAPLE*. However, *STAPLE* requires 'good quality' segmented geometries. For example, one of the patients under study (KGC4) had a hip prosthesis which induced the *STAPLE* algorithms in error. The femur's head was not recognized as the femur's most distal point, thus causing the inversion of the hip and knee joints' location. Regarding muscle registration, according to Scheys et al., (2006), the definition of the lower limb muscle pathways using a semi-automatic method, similar to the proposed pipeline, took 65 min on average. Similarly, in this work, the muscle–tendon pathways were generated, on average, in 60 min: 30 min to define the muscle points and 30 min to add the wrapping surfaces. Nonetheless, it must be noted that an additional 30 min was required, before the muscle registration, to prepare the generic model. Indeed, the mapping procedure was achieved by correctly identifying, adding and extracting a complete set of anatomical bony landmarks of the generic model to properly guide the

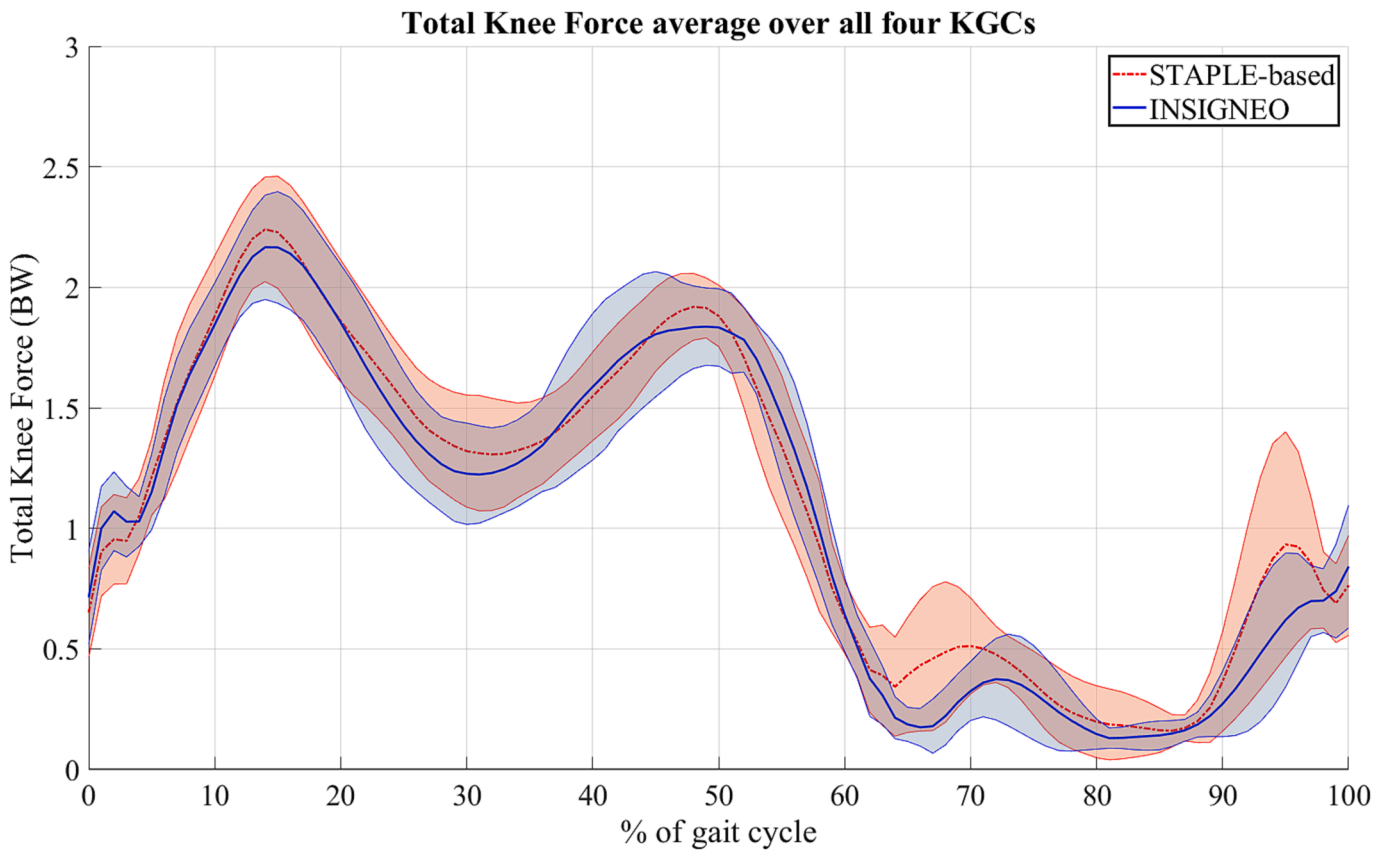

Fig. 2. Mean (line) and standard deviation (shaded area) of the predicted total knee contact force computed with the *INSIGNEO* (blue) and the *STAPLE*-based (red) pipeline, expressed in body weight (BW), averaged across the 19 trials of the models generated. (For interpretation of the references to colour in this figure legend, the reader is referred to the web version of this article.)

single-value decomposition algorithm. This process was, however, performed only once, not on every patient. Therefore, a complete MSK model was generated on average in around 60 min with the proposed *STAPLE*-based pipeline, compared to an average of 160 min with the *INSIGNEO* pipeline. The 65 %-time reduction required to develop an image-based MSK model, using the semi-automated *STAPLE*-based pipeline, opens up the possibility to use subject-specific MSK models as a tool for large-scale clinical studies.

The current study has some limitations. First, a number of idealizations were made to build the subject-specific MSK models. For instance, the generic Full Body model (Rajagopal et al., 2016), used as a reference model, is representative of a healthy young individual. In addition, since the only available medical images were CT scans, it was difficult to distinguish between muscle and fat inclusions. However, care was taken to personalize the muscle properties as best as possible. The maximal isometric forces were personalized using the CT scans and muscle volumes extracted from the literature (Montefiori et al., 2020), and the muscle lengths were morphometrically optimized using the implementation of Modenese et al., (2016). Finally, no intra- and inter-operator variability was assessed. Nonetheless, it has already been shown that the sensitivity of model outcomes to uncertainty in joint forces tends to be less than 0.33BW (i.e., less than 10 % of the peak joint contact force) for hip, knee and ankle joints (Martelli et al., 2015), and to induce a maximum standard deviation of 0.26BW across the stance phase of gait (Valente et al., 2014).

In conclusion, the models produced similar results, irrespective of the pipeline used, but with a drastic time reduction in generating MSK models with the *STAPLE*-based pipeline. The ability to create a subject-specific model of MSK dynamics in around 60 min opens up the possibility of using these models to non-invasively estimate joint forces in patients enrolled in phase III clinical studies.

CRediT authorship contribution statement

Domitille Princelle: Conceptualization, Data curation, Writing - original draft, Writing - review & editing, Formal analysis, Methodology. **Giorgio Davico:** Conceptualization, Writing - review & editing. **Marco Viceconti:** Conceptualization, Funding acquisition, Writing - review & editing, Supervision, Project administration.

Declaration of Competing Interest

The authors declare that they have no known competing financial interests or personal relationships that could have appeared to influence the work reported in this paper.

Data availability

The models, data (processed and interpolated), and supplementary figures and material used in this study are available in the University of Bologna institutional repository under the CC BY 4.0 international license terms at the link http://amsacta.unibo.it/id/eprint/7153.

Acknowledgement

This study was supported by the European Commission through the H2020 project "In Silico World: Lowering barriers to ubiquitous adoption of In Silico Trials" (topic SC1-DTH-06-2020, grant ID 101016503). The authors declare no conflicts of interest.

Annex 1.

The anatomical markers landmarks were automatically generated in *STAPLE* and compared to the landmarks manually identified in *INSIGNEO*

Rigid body	Description of Body landmark
Pelvis	Right anterior superior iliac spine
	Left anterior superior iliac spine
	Right posterior superior iliac spine
	Left posterior iliac spine
Femur	Great trochanter
	Lateral femoral epicondyle
	Medial femoral epicondyle
Tibia/Fibula	Tibial tuberosity
	Fibula head
	Medial malleolus
	Lateral malleolus
Foot	Heel
	Head of fifth metatarsal bone
	Head of first metatarsal bone

Comparison between the point clouds automatically (*STAPLE*) and manually (*INSIGNEO*) identified. Specifically, the RMSE, the maximal and minimal distances (mm) between corresponding markers of both pipelines were calculated: for both anatomical and muscle landmarks.

KGC	Landmark		Distance (mm)	Marker
KGC3	Anatomical	RMSE	7.2 ± 3.9	
		Min	<0.1	TTB: Tibial tuberosity
		Max	13.4	Knee Medial
	Muscle	RMSE	3.5 ± 3.8	
		Min	<0.1	4 Muscle points (e.g., tibialis posterior muscle origin)
		Max	17.2	extensor digitorum longus (path point)
KGC4	Anatomical	RMSE	6.1 ± 3.1	
		Min	1.3	D5M: Head of 5th metatarsal
		Max	10.9	Knee Lateral
	Muscle	RMSE	2.6 ± 3.1	
		Min	<0.1	23 Muscle points (e.g., Extensor Hallucis Longus via points and insertion)
		Max	20.2	Sartorius (origin)
KGC5	Anatomical	RMSE	7.2 ± 3.0	
		Min	1.8	Knee Lateral
		Max	11.6	LPsis (pelvis)
	Muscle	RMSE	3.3 ± 3.0	
		Min	<0.1	5 Muscle points (e.g., Semimembranosus insertion)
		Max	10.8	Rectus femoris (path point)
KGC6	Anatomical	RMSE	7.9 ± 3.4	
		Min	1.3	TRO: Great trochanter
		Max	13.4	LPsis (pelvis)
	Muscle	RMSE	4.2 ± 4.5	
		Min	<0.1	14 Muscle points (e.g., Quadriceps insertion)
		Max	21.2	Piriformis (origin)

Appendix A. Supplementary material

Supplementary data to this article can be found online at https://doi.org/10.1016/j.jbiomech.2023.111758.

References

Anderson, F.C., Pandy, M.G., 2001. Static and dynamic optimization solutions for gait are practically equivalent. J. Biomech. 34, 153–161. https://doi.org/10.1016/S0021-9290(00)00155-X.

Arnold, A.S., Salinas, S., Hakawa, D.J., Delp, S.L., 2000. Accuracy of muscle moment arms estimated from MRI-based musculoskeletal models of the lower extremity. Comput. Aided Surg. 5, 108–119. https://doi.org/10.3109/10929080009148877.

Arnold, E.M., Ward, S.R., Lieber, R.L., Delp, S.L., 2010. A model of the lower limb for analysis of human movement. Ann. Biomed. Eng. 38, 269–279. https://doi.org/10.1007/s10439-009-9852-5.

Barber, L., Carty, C., Modenese, L., Walsh, J., Boyd, R., Lichtwark, G., 2017. Medial gastrocnemius and soleus muscle-tendon unit, fascicle, and tendon interaction during walking in children with cerebral palsy. Dev. Med. Child Neurol. 59, 843–851. https://doi.org/10.1111/dmcn.13427.

Barzan, M., Modenese, L., Carty, C.P., Maine, S., Stockton, C.A., Sancisi, N., Lewis, A., Grant, J., Lloyd, D.G., Brito da Luz, S., 2019. Development and validation of subject-specific pediatric multibody knee kinematic models with ligamentous constraints. J. Biomech. 93, 194–203. https://doi.org/10.1016/j.jbiomech.2019.07.001.

Bennett, K.J., Pizzolato, C., Martelli, S., Bahl, J.S., Sivakumar, A., Atkins, G.J., Solomon, L.B., Thewlis, D., 2022. EMG-informed neuromusculoskeletal models accurately predict knee loading measured using instrumented implants. IEEE Trans. Biomed. Eng. 1 https://doi.org/10.1109/TBME.2022.3141067.

Bergmann, G., Deuretzbacher, G., Heller, M., Graichen, F., Rohlmann, A., Strauss, J., Duda, G.N., 2001. Hip contact forces and gait patterns from routine activities. J. Biomech. 34, 859–871. https://doi.org/10.1016/S0021-9290(01)00040-9.

Brand, R.A., Pedersen, D.R., Davy, D.T., Kotzar, G.M., Heiple, K.G., Goldberg, V.M., 1994. Comparison of hip force calculations and measurements in the same patient. J. Arthroplasty 9, 45–51. https://doi.org/10.1016/0883-5403(94)90136-8.

Bull, A.M.J., Reilly, P., Wallace, A.L., Amis, A.A., Emery, R.J.H., 2005. A novel technique to measure active tendon forces: application to the subscapularis tendon. Knee Surg. Sports Traumatol. Arthrosc. 13, 145–150. https://doi.org/10.1007/s00167-004-0556-y.

Carbone, V., Fluit, R., Pellikaan, P., van der Krogt, M.M., Janssen, D., Damsgaard, M., Vigneron, L., Feilkas, T., Koopman, H.F.J.M., Verdonschot, N., 2015. TLEM 2.0 – a comprehensive musculoskeletal geometry dataset for subject-specific modeling of lower extremity. J. Biomech. 48, 734–741. https://doi.org/10.1016/j.jbiomech.2014.12.034.

Correa, T.A., Baker, R., Kerr Graham, H., Pandy, M.G., 2011. Accuracy of generic musculoskeletal models in predicting the functional roles of muscles in human gait. J. Biomech. 44, 2096–2105. https://doi.org/10.1016/j.jbiomech.2011.05.023.

Crowninshield, R.D., Brand, R.A., 1981. A physiologically based criterion of muscle force prediction in locomotion. J. Biomech. 14, 793–801. https://doi.org/10.1016/0021-9290(81)90035-X.

Davico, G., Pizzolato, C., Killen, B.A., Barzan, M., Suwarganda, E.K., Lloyd, D.G., Carty, C.P., 2020a. Best methods and data to reconstruct paediatric lower limb bones for musculoskeletal modelling. Biomech. Model. Mechanobiol. 19, 1225–1238. https://doi.org/10.1007/s10237-019-01245-y.

Davico, G., Pizzolato, C., Lloyd, D.G., Obst, S.J., Walsh, H.P.J., Carty, C.P., 2020b. Increasing level of neuromusculoskeletal model personalisation to investigate joint contact forces in cerebral palsy: a twin case study. Clin. Biomech. 72, 141–149. https://doi.org/10.1016/j.clinbiomech.2019.12.011.

Delp, S.L., Loan, J.P., Hoy, M.G., Zajac, F.E., Topp, E.L., Rosen, J.M., 1990. An interactive graphics-based model of the lower extremity to study orthopaedic surgical procedures. IEEE Trans. Biomed. Eng. 37, 757–767. https://doi.org/10.1109/10.102791.

Delp, S.L., Anderson, F.C., Arnold, A.S., Loan, P., Habib, A., John, C.T., Guendelman, E., Thelen, D.G., 2007. OpenSim: open-source software to create and analyze dynamic simulations of movement. IEEE Trans. Biomed. Eng. 54, 1940–1950. https://doi.org/10.1109/TBME.2007.901024.

Dumas, R., Aissaoui, R., Mitton, D., Skalli, W., deGuise, J.A., 2005. Personalized body segment parameters from biplanar low-dose radiography. IEEE Trans. Biomed. Eng. 52, 1756–1763. https://doi.org/10.1109/TBME.2005.855711.

Erdemir, A., McLean, S., Herzog, W., van den Bogert, A.J., 2007. Model-based estimation of muscle forces exerted during movements. Clin. Biomech. 22, 131–154. https://doi.org/10.1016/j.clinbiomech.2006.09.005.

Falisse, A., Pitto, L., Kainz, H., Hoang, H., Wesseling, M., Van Rossom, S., Papageorgiou, E., Bar-On, L., Hallemans, A., Desloovere, K., Molenaers, G., Van Campenhout, A., De Groote, F., Jonkers, I., 2019. Physics-based predictive simulations to explore the differential effects of motor control and musculoskeletal deficits on gait dysfunction in cerebral palsy: a retrospective case study. Bioengineering. https://doi.org/10.1101/769042 (preprint).

Finni, T., Komi, P.V., Lukkariniemi, J., 1998. Achilles tendon loading during walking: application of a novel optic fiber technique. Eur. J. Appl. Physiol. 77, 289–291. https://doi.org/10.1007/s004210050335.

Fraysse, F., Dumas, R., Cheze, L., Wang, X., 2009. Comparison of global and joint-to-joint methods for estimating the hip joint load and the muscle forces during walking. J. Biomech. 42, 2357–2362. https://doi.org/10.1016/j.jbiomech.2009.06.056.

Fregly, B.J., Besier, T.F., Lloyd, D.G., Delp, S.L., Banks, S.A., Pandy, M.G., D'Lima, D.D., 2012. Grand challenge competition to predict in vivo knee loads: GRAND CHALLENGE COMPETITION. J. Orthop. Res. 30, 503–513. https://doi.org/10.1002/jor.22023.

Garner, B.A., Pandy, M.G., 2001. Musculoskeletal model of the upper limb based on the visible human male dataset. Comput. Methods Biomech. Biomed. Eng. 4, 93–126. https://doi.org/10.1080/10255840008908000.

Gerus, P., Sartori, M., Besier, T.F., Fregly, B.J., Delp, S.L., Banks, S.A., Pandy, M.G., D'Lima, D.D., Lloyd, D.G., 2013. Subject-specific knee joint geometry improves predictions of medial tibiofemoral contact forces. J. Biomech. 46, 2778–2786. https://doi.org/10.1016/j.jbiomech.2013.09.005.

Hamner, S.R., Seth, A., Delp, S.L., 2010. Muscle contributions to propulsion and support during running. J. Biomech. 43, 2709–2716. https://doi.org/10.1016/j.jbiomech.2010.06.025.

Horn, B.K.P., 1987. Closed-form solution of absolute orientation using unit quaternions. J. Opt. Soc. Am. A 4, 629. https://doi.org/10.1364/JOSAA.4.000629.

Kai, S., Sato, T., Koga, Y., Omori, G., Kobayashi, K., Sakamoto, M., Tanabe, Y., 2014. Automatic construction of an anatomical coordinate system for three-dimensional bone models of the lower extremities – Pelvis, femur, and tibia. J. Biomech. 47, 1229–1233. https://doi.org/10.1016/j.jbiomech.2013.12.013.

Kainz, H., Modenese, L., Lloyd, D.G., Maine, S., Walsh, H.P.J., Carty, C.P., 2016. Joint kinematic calculation based on clinical direct kinematic versus inverse kinematic gait models. J. Biomech. 49, 1658–1669. https://doi.org/10.1016/j.jbiomech.2016.03.052.

Killen, B.A., Brito da Luz, S., Lloyd, D.G., Carleton, A.D., Zhang, J., Besier, T.F., Saxby, D. J., 2021. Automated creation and tuning of personalised muscle paths for OpenSim musculoskeletal models of the knee joint. Biomech. Model. Mechanobiol. 20, 521–533. https://doi.org/10.1007/s10237-020-01398-1.

Kim, H.J., Fernandez, J.W., Akbarshahi, M., Walter, J.P., Fregly, B.J., Pandy, M.G., 2009. Evaluation of predicted knee-joint muscle forces during gait using an instrumented knee implant. J. Orthop. Res. 27, 1326–1331. https://doi.org/10.1002/jor.20876.

Klein Horsman, M.D., 2007. The Twente lower extremity model: consistent dynamic simulation of the human locomotor apparatus. s.n. S.l.

Komi, P.V., Fukashiro, S., Järvinen, M., 1992. Biomechanical loading of Achilles tendon during normal locomotion. Clin. Sports Med. 11, 521–531. https://doi.org/10.1016/S0278-5919(20)30506-8.

Lenaerts, G., De Groote, F., Demeulenaere, B., Mulier, M., Van der Perre, G., Spaepen, A., Jonkers, I., 2008. Subject-specific hip geometry affects predicted hip joint contact forces during gait. J. Biomech. 41, 1243–1252. https://doi.org/10.1016/j.jbiomech.2008.01.014.

Lerner, Z.F., DeMers, M.S., Delp, S.L., Browning, R.C., 2015. How tibiofemoral alignment and contact locations affect predictions of medial and lateral tibiofemoral contact forces. J. Biomech. 48, 644–650. https://doi.org/10.1016/j.jbiomech.2014.12.049.

Lu, T.-W., O'Connor, J.J., 1999. Bone position estimation from skin marker co-ordinates using global optimisation with joint constraints. J. Biomech. 32, 129–134. https://doi.org/10.1016/S0021-9290(98)00158-4.

Mantoan, A., Pizzolato, C., Sartori, M., Sawacha, Z., Cobelli, C., Reggiani, M., 2015. MOtoNMS: a MATLAB toolbox to process motion data for neuromusculoskeletal modeling and simulation. Source Code Biol. Med. 10, 12. https://doi.org/10.1186/s13029-015-0044-4.

Marra, M.A., Vanheule, V., Fluit, R., Koopman, B.H.F.J.M., Rasmussen, J., Verdonschot, N., Andersen, M.S., 2015. A subject-specific musculoskeletal modeling framework to predict in vivo mechanics of total knee arthroplasty. J. Biomech. Eng. 137, 020904 https://doi.org/10.1115/1.4029258.

Martelli, S., Taddei, F., Cappello, A., van Sint Jan, S., Leardini, A., Viceconti, M., 2011. Effect of sub-optimal neuromotor control on the hip joint load during level walking. J. Biomech. 44, 1716–1721. https://doi.org/10.1016/j.jbiomech.2011.03.039.

Martelli, S., Valente, G., Viceconti, M., Taddei, F., 2015. Sensitivity of a subject-specific musculoskeletal model to the uncertainties on the joint axes location. Comput. Methods Biomech. Biomed. Eng. 18, 1555–1563. https://doi.org/10.1080/10255842.2014.930134.

Modenese, L., Ceseracciu, E., Reggiani, M., Lloyd, D.G., 2016. Estimation of musculotendon parameters for scaled and subject specific musculoskeletal models using an optimization technique. J. Biomech. 49, 141–148. https://doi.org/10.1016/j.jbiomech.2015.11.006.

Modenese, L., Montefiori, E., Wang, A., Wesarg, S., Viceconti, M., Mazzà, C., 2018. Investigation of the dependence of joint contact forces on musculotendon parameters using a codified workflow for image-based modelling. J. Biomech. 73, 108–118. https://doi.org/10.1016/j.jbiomech.2018.03.039.

Modenese, L., Renault, J.-B., 2021. Automatic generation of personalised skeletal models of the lower limb from three-dimensional bone geometries. J. Biomech. 116, 110186 https://doi.org/10.1016/j.jbiomech.2020.110186.

Montefiori, E., Modenese, L., Di Marco, R., Magni-Manzoni, S., Malattia, C., Petrarca, M., Ronchetti, A., de Horatio, L.T., van Dijkhuizen, P., Wang, A., Wesarg, S., Viceconti, M., Mazzà, C., 2019. An image-based kinematic model of the tibiotalar and subtalar joints and its application to gait analysis in children with Juvenile Idiopathic Arthritis. J. Biomech. 85, 27–36. https://doi.org/10.1016/j.jbiomech.2018.12.041.

Montefiori, E., Kalkman, B.M., Henson, W.H., Paggiosi, M.A., McCloskey, E.V., Mazzà, C., Rushton, A., 2020. MRI-based anatomical characterisation of lower-limb muscles in older women. PLoS ONE 15 (12), e0242973. https://doi.org/10.1371/journal.pone.0242973.

Morrison, J.B., 1970. The mechanics of the knee joint in relation to normal walking. J. Biomech. 3, 51–61. https://doi.org/10.1016/0021-9290(70)90050-3.

Nardini, F., Belvedere, C., Sancisi, N., Conconi, M., Leardini, A., Durante, S., Parenti-Castelli, V., 2020. An anatomical-based subject-specific model of in-vivo knee joint 3D kinematics from medical imaging. Appl. Sci. 10, 2100 https://doi.org/10.3390/app10062100.

Pedersen, D.R., Brand, R.A., Davy, D.T., 1997. Pelvic muscle and acetabular contact forces during gait. J. Biomech. 30, 959–965. https://doi.org/10.1016/S0021-9290(97)00041-9.

Rajagopal, A., Dembia, C.L., DeMers, M.S., Delp, D.D., Hicks, J.L., Delp, S.L., 2016. Full-body musculoskeletal model for muscle-driven simulation of human gait. IEEE Trans. Biomed. Eng. 63, 2068–2079. https://doi.org/10.1109/TBME.2016.2586891.

Renault, J.-B., Aüllo-Rasser, G., Donnez, M., Parratte, S., Chabrand, P., 2018. Articular-surface-based automatic anatomical coordinate systems for the knee bones. J. Biomech. 80, 171–178. https://doi.org/10.1016/j.jbiomech.2018.08.028.

Saxby, D.J., Modenese, L., Bryant, A.L., Gerus, P., Killen, B., Fortin, K., Wrigley, T.V., Bennell, K.L., Cicuttini, F.M., Lloyd, D.G., 2016. Tibiofemoral contact forces during walking, running and sidestepping. Gait Posture 49, 78–85. https://doi.org/10.1016/j.gaitpost.2016.06.014.

Scheys, L., Jonkers, I., Loeckx, D., Maes, F., Spaepen, A., Suetens, P., 2006. Image based musculoskeletal modeling allows personalized biomechanical analysis of gait. In: Harders, M., Székely, G. (Eds.), Biomedical Simulation, Lecture Notes in Computer Science. Springer Berlin Heidelberg, Berlin, Heidelberg, pp. 58–66. doi: 10.1007/11790273_7.

Scheys, L., Jonkers, I., Schutyser, F., Pans, S., Spaepen, A., Suetens, P., 2005. Image based methods to generate subject-specific musculoskeletal models for gait analysis. Int. Congr. Ser. 1281, 62–67. https://doi.org/10.1016/j.ics.2005.03.076.

Scheys, L., Van Campenhout, A., Spaepen, A., Suetens, P., Jonkers, I., 2008. Personalized MR-based musculoskeletal models compared to rescaled generic models in the presence of increased femoral anteversion: effect on hip moment arm lengths. Gait Posture 28, 358–365. https://doi.org/10.1016/j.gaitpost.2008.05.002.

Seireg, A., Arvikar, R.J., 1973. A mathematical model for evaluation of forces in lower extremeties of the musculo-skeletal system. J. Biomech. 6, 313–326. https://doi.org/10.1016/0021-9290(73)90053-5.

Seth, A., Hicks, J.L., Uchida, T.K., Habib, A., Dembia, C.L., Dunne, J.J., Ong, C.F., DeMers, M.S., Rajagopal, A., Millard, M., Hamner, S.R., Arnold, E.M., Yong, J.R., Lakshmikanth, S.K., Sherman, M.A., Ku, J.P., Delp, S.L., Schneidman, D., 2018. OpenSim: simulating musculoskeletal dynamics and neuromuscular control to study human and animal movement. PLoS Comput. Biol. 14 (7), e1006223 https://doi.org/10.1371/journal.pcbi.1006223.

Suwarganda, E.K., Diamond, L.E., Lloyd, D.G., Besier, T.F., Zhang, J.u., Killen, B.A., Savage, T.N., Saxby, D.J., Livesu, M., 2019. Minimal medical imaging can accurately reconstruct geometric bone models for musculoskeletal models. PLoS ONE 14 (2), e0205628. https://doi.org/10.1371/journal.pone.0205628.

Taddei, F., Martelli, S., Valente, G., Leardini, A., Benedetti, M.G., Manfrini, M., Viceconti, M., 2012. Femoral loads during gait in a patient with massive skeletal reconstruction. Clin. Biomech. 27, 273–280. https://doi.org/10.1016/j.clinbiomech.2011.09.006.

Taylor, W.R., Heller, M.O., Bergmann, G., Duda, G.N., 2004. Tibio-femoral loading during human gait and stair climbing. J. Orthop. Res. 22, 625–632. https://doi.org/10.1016/j.orthres.2003.09.003.

Taylor, W.R., Schütz, P., Bergmann, G., List, R., Postolka, B., Hitz, M., Dymke, J., Damm, P., Duda, G., Gerber, H., Schwachmeyer, V., Hosseini Nasab, S.H., Trepczynski, A., Kutzner, I., 2017. A comprehensive assessment of the musculoskeletal system: The CAMS-Knee data set. J. Biomech. 65, 32–39. https://doi.org/10.1016/j.jbiomech.2017.09.022.

Thelen, D.G., Won Choi, K., Schmitz, A.M., 2014. Co-simulation of neuromuscular dynamics and knee mechanics during human walking. J. Biomech. Eng. 136, 021033 https://doi.org/10.1115/1.4026358.

Valente, G., Pitto, L., Testi, D., Seth, A., Delp, S.L., Stagni, R., Viceconti, M., Taddei, F., Soncini, M., 2014. Are subject-specific musculoskeletal models robust to the uncertainties in parameter identification? PLoS ONE 9 (11), e112625. https://doi.org/10.1371/journal.pone.0112625.

Valente, G., Crimi, G., Vanella, N., Schileo, E., Taddei, F., 2017. nmsBuilder: freeware to create subject-specific musculoskeletal models for OpenSim. Comput. Methods Programs Biomed. 152, 85–92. https://doi.org/10.1016/j.cmpb.2017.09.012.

Viceconti, M., Ascani, D., Mazzà, C., 2019. Pre-operative prediction of soft tissue balancing in knee arthoplasty part 1: effect of surgical parameters during level walking. J. Orthop. Res. 37, 1537–1545. https://doi.org/10.1002/jor.24289.

Ward, S.R., Eng, C.M., Smallwood, L.H., Lieber, R.L., 2009. Are current measurements of lower extremity muscle architecture accurate? Clin. Orthop. 467, 1074–1082. https://doi.org/10.1007/s11999-008-0594-8.

Wesseling, M., De Groote, F., Bosmans, L., Bartels, W., Meyer, C., Desloovere, K., Jonkers, I., 2016. Subject-specific geometrical detail rather than cost function formulation affects hip loading calculation. Comput. Methods Biomech. Biomed. Eng. 19, 1475–1488. https://doi.org/10.1080/10255842.2016.1154547.

White, D.R., Woodard, H.Q., Hammond, S.M., 1987. Average soft-tissue and bone models for use in radiation dosimetry. Br. J. Radiol. 60, 907–913. https://doi.org/10.1259/0007-1285-60-717-907.

Wu, G., Siegler, S., Allard, P., Kirtley, C., Leardini, A., Rosenbaum, D., Whittle, M., D'Lima, D.D., Cristofolini, L., Witte, H., Schmid, O., Stokes, I., 2002. ISB recommendation on definitions of joint coordinate system of various joints for the reporting of human joint motion—part I: ankle, hip, and spine. J. Biomech. 35, 543–548. https://doi.org/10.1016/S0021-9290(01)00222-6.

Zhang, J., Sorby, H., Clement, J., Thomas, C.D.L., Hunter, P., Nielsen, P., Lloyd, D., Taylor, M., Besier, T., 2014. The MAP Client: user-friendly musculoskeletal modelling workflows. In: Bello, F., Cotin, S. (Eds.), Biomedical Simulation, Lecture Notes in Computer Science. Springer International Publishing, Cham, pp. 182–192. doi: 10.1007/978-3-319-12057-7_21.